DrillBit
Anti Plagiarism Software

The Report is Generated by DrillBit Plagiarism Detection Software

Submission Information

Author Name	Srajan-Yash
Title	ISR2
Submission/Paper ID	360745
Submission Date	17-Aug-2021 12:38:55
Total Pages	15
Total Words	2541

Result Information

Similarity	15 %
Unique	85 %
Internet Sources	2 %
Journal/Publication Sources	13 %

Exclude Information

References/Bibliography	Excluded
Quotes	Excluded
Sources: Less than 14 Words Similarity	Excluded

DrillBit
Anti Plagiarism Software

DrillBit Similarity Report

15	24	B
SIMILARITY %	MATCHED SOURCES	GRADE

A-Satisfactory (0-10%)
B-Upgrade (11-40%)
C-Poor (41-60%)
D-Unacceptable (61-100%)

Sl.No	LOCATION	MATCHED DOMAIN	%	SOURCE TYPE
1.	1	citeseerx.ist.psu.edu	4	Publication
2.	15	www.sciencedirect.com	2	Internet
3.	6	ocw.mit.edu	2	Publication
4.	19	Numerical Simulation of the Turbulent Flow in Ultra-Precision Aerostatic Bearing by Zhu-2013	<1	Publication
5.	14	Flow visualisation studies of aerodynamic characteristics of an open-top chamber by Schmitt-1987	<1	Publication.
6.	7	Review of numerical simulations for high-speed, turbulent cavity flows by SJ-2011	<1	Publication
7.	12	American Institute of Aeronautics and Astronautics 24th Aerospace Sc	<1	Publication
8.	2	Experimental and numerical investigation of a freefall wedge vertically entering by Wang-2015	<1	Publication

9.	4	Forward Modeling Time-Lapse Seismic based on Reservoir Simulation Resu by Asikin-2017	<1	Publication
10.	17	Flow around a cylinder surrounded by a permeable cylinder in shallow w by Goktur-2012	<1	Publication
11.	16	Synchronization of fractional order chaotic systems using active cont, by S.K. Agrawal M. Sr- 2012	<1	Publication
12.	10	Review of cavity ignition in supersonic flows by Cai-2019	<1	Publication
13.	21	Step-frequency operation of a coaxial cavity gyrotron from 134 to 169 by Piosczyk-2000	<1	Publication
14.	20	IEEE 2015 18th International Conference on Intelligent System Applic by	<1	Publication
15.	8	American Institute of Aeronautics and Astronautics 46th AIAAASMESA	<1	Publication
16.	5	Feasibility Analysis of Reverse Sealed Testing String in HPHT Wells by Gao-2014	<1	Publication
17.	3	A novel automated course generation system embedded in the online lecturing plat by Osamnia-2016	<1	Publication
18.	23	Improvement of cavity shape modeling in water-entry of circular cylind by Mirzaei-2020	<1	Publication

19.	22	Female-produced sexual pheromone ofSceliodes cordalis(Lepidoptera Pyr by J-1986	<1	Publication
20.	18	American Institute of Aeronautics and Astronautics 40th Fluid Dynami	<1	Publication
21.	13	Paper published at International Journal of Engineering & Technology - www.sciencepubco.com	<1	Publication
22.	11	American Institute of Aeronautics and Astronautics 5th AIAACEAS Aer	<1	Publication
23.	9	AUTHOR INDEX Volume 24,- 2010	<1	Publication
24.	24	A single product perishable inventory system with compulsory waiting period for by Yadavalli-2018	<1	Publication

ABSTRACT

Numerical simulations were done to obtain flow field around a cavity at various angles of attack (α) at 2.0 Mach number of length-to-depth ratios (L/D) of 1.0 and 3.0. Unsteady, planar and two-dimensional simulations were done using ANSYS FLUENT. Pressure distribution on the upper cavity as well as lower cavity were obtained. Simulations done on the back wall of the cavity shows that pressure fluctuations of periodic oscillations occur in L/D = 1 but are non-periodic in nature in case of L/D = 3. The obtained results shows that the pressure distribution remains almost constant in upper section and lower section of cavity except for its magnitude. In comparison to lower cavity, upper cavity has lower pressure and the angle of attack is increased as the difference in these value of pressure increases.

INTRODUCTION

Axisymmetric cavities are the annular rectangular section on a body of revolution. High speed flows inside cavities have many applications in aerospace sector including carriage and release of payloads and armaments, landing gears, supersonic flow mixing and flame holding devices in scramjet engines. The propulsion system in the scramjet engines requires rapid mixing of hydrogen fuel and atmospheric air for efficient combustion and also to minimize the size of combustion chamber. Cavity flow comprises a complex unsteadiness, pressure fluctuations and high resonance. Separation of turbulent boundary layer, vortices and shear surface instabilities also occur in supersonic cavity flows. Complications arise from pressure fluctuations that are produced by the flow past the open cavity which can cause instrument failure, structural fatigue, damage to the stores, and increase in aerodynamic loading etc. It can also create negative effects on the stable release of payloads and armaments and their trajectories.

There are numerous ways to classify the cavity flow field based upon L/D and L/W ratio, Mach number, Reynolds number and in accordance with oscillation mechanism. L/W ratio is not applicable when we talk about axisymmetric cavity. Usually, axisymmetric cavity is classified on the basis of basic flow field inside the cavity and geometry of the cavity, i.e., 'Open', 'Closed' and 'Transitional'.

Open Cavity: These cavities are short, deep and has L/D ratio less than 10. Oscillating shear layer disconnects from the front wall of cavity, bridges the length of cavity and connects on the corner of the back wall of cavity.

Closed Cavity: Shallow cavities with L/D ratio larger than 13 can be categorized as closed cavities. In closed cavity flow, the flow separates at the front wall of the cavity, reattaches at some point along the base of cavity, and segregates again before reaching the rear wall of cavity.

Transitional Cavity: Cavities with L/D ratio between 10 and 13 are known as transitional cavity. Basically, there is transitional type of flow, i.e., flow is changing from open cavity type to closed cavity type.

In this project, an attempt has been made to simulate the flow field over axisymmetric cavity with L/D = 1 and 3, at Mach number of 2.0. The angle of attack of the cavity was varied and its consequence on peak pressure and pressure fluctuations on the back wall corner of the cavity has been analyzed.

The axisymmetric cavity model consists of conical fore-body having 12° semi-cone angle, Length (L) of the cavity was maintained as 4mm and 12mm and depth (D) as 4 mm. The maximum exterior diameter (De) of the model happened to be 15mm. Effects of three different angle of attacks of α = 3°, 5°, 10° were studied in this project.

VALIDATION TEST

For the purpose of validation, simulation was done on the cavity of L/D = 1.33 at Mach 2.2 and results were verified from [1] and [2] by comparing the distribution of static pressure inside the cavity. Present computation results and the results of the mentioned references were in good agreement. Therefore, a similar grid and FLUENT setup settings were used to perform further simulations. Pressure distribution curve from [1], [2] and present computations are presented in below figures. Here $0 \leq s/D \leq 1$ corresponds to the front-wall of the cavity, $1 \leq s/D \leq 2.33$ is the base of the cavity and $2.33 \leq s/D \leq 3.33$ is the back wall of cavity.

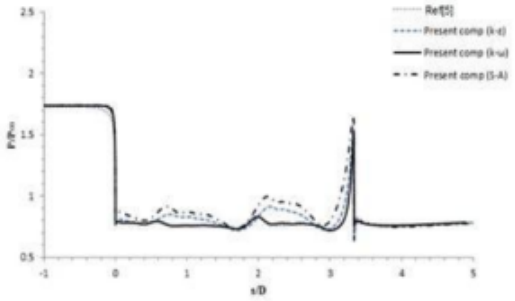

Fig. 1: Pressure Distribution for L/D = 1.33 at Mach 2.2 from Ref [1]

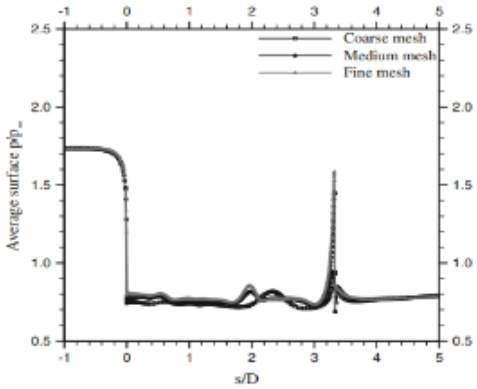

Fig. 2: Pressure Distribution for L/D = 1.33 at Mach 2.2 from Ref [2]

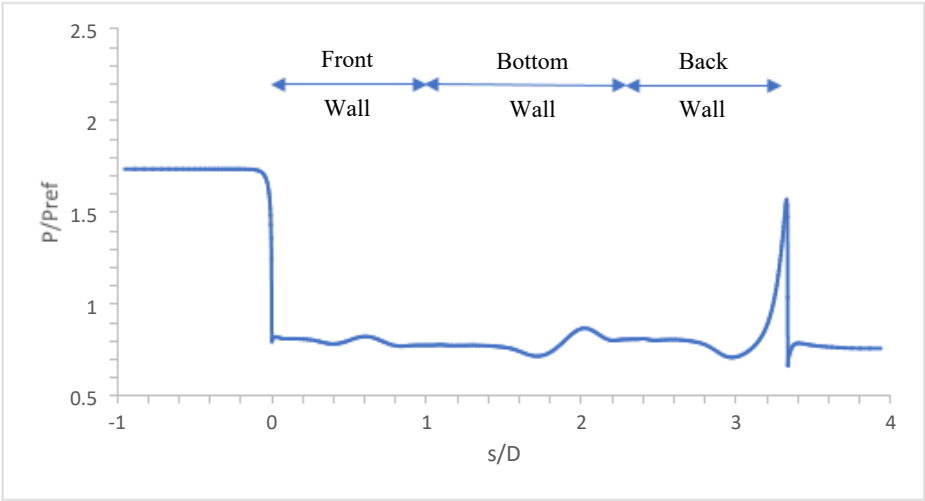

Fig. 3: Pressure Distribution for L/D = 1.33 at Mach 2.2 with present computations

COMPUTATIONS

Planar, unsteady and two-dimensional simulations were made using a commercial CFD software FLUENT to acquire the flow field inside and around the cavity at different angles of attack of 3°, 5° and 10°. A coupled solver adopting k-ω SST turbulence model with 2nd order implicit time and space stepping was employed. Time step size was taken as 1e-05 and courant number as 0.8 to capture periodic oscillations of pressure on the rear wall of cavity. Solution convergence was established by monitoring residuals of density, velocities, turbulent kinetic energy (k) and specific rate of dissipation (ω) and monitoring pressure at a specific point on the rear wall of cavity.

Structured meshing was done with Mesh tool in ANSYS workbench in case of L/D = 3. But in case of L/D = 1, structured meshing was done using GAMBIT. Suitable edge biasing was done to generate the flow field inside and around the cavity. The distance of first cell from the cavity wall was 0.005 mm.

An axisymmetric, unsteady and two-dimensional simulations were also accomplished for L/D = 3 at 0° angle of attack and Mach number 2.0 for validation purposes. A good agreement can be seen for results obtained through standard k- ω turbulence model. Hence further computations were made keeping similar turbulent model and grids for the present cavity geometries and cases.

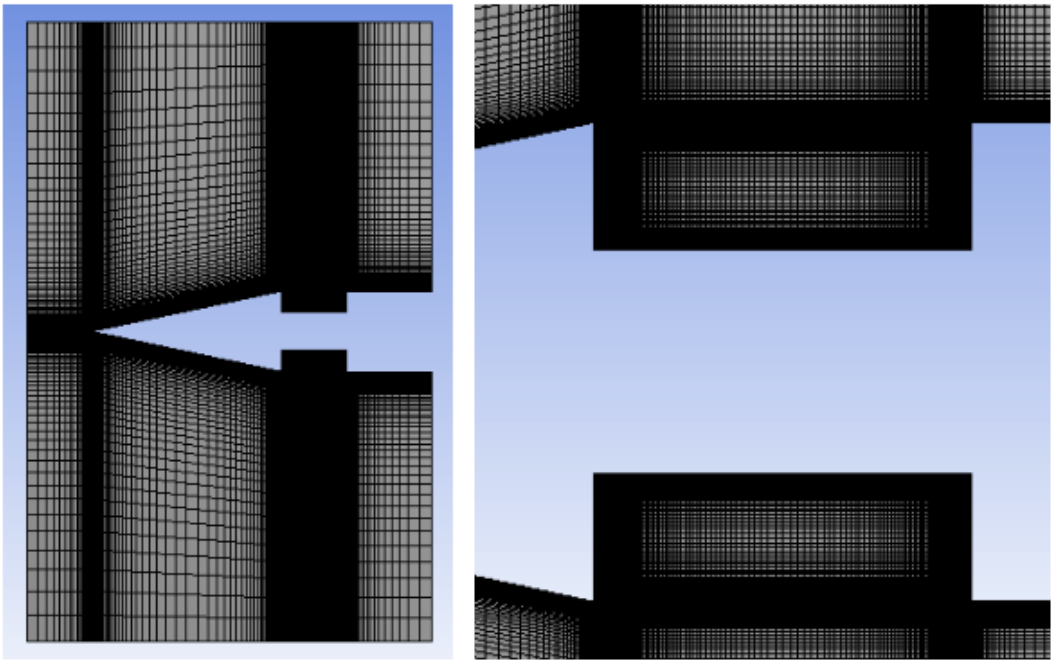

(a) **(b)**

Fig. 4: (a) Structured Meshing for L/D = 3. **(b)** Structured Meshing inside cavity.

RESULTS AND DISCUSSIONS

Simulations were initially performed to generate the flow field around an axisymmetric cavity of L/D = 3. Mach contour, pressure distribution, pressure contour and density contour are shown underneath. It can be observed that a subsonic recirculatory flow is formed inside the cavity. A smaller recirculatory zone behind the main zone is also formed which further excited the shear layer above it resulting in higher peak pressure on the back wall corner of the cavity in comparison with the cavity of L/D = 1. The corresponding mean static pressure distribution is also presented in Fig. 3, where 0<s/D<1 represents front wall surface, 1<s/D<4 represents cavity bottom surface and 4<s/D<5 represents cavity rear wall. A peak pressure of around 1.35 is detected at the tip of the back wall which represents the compression wave.

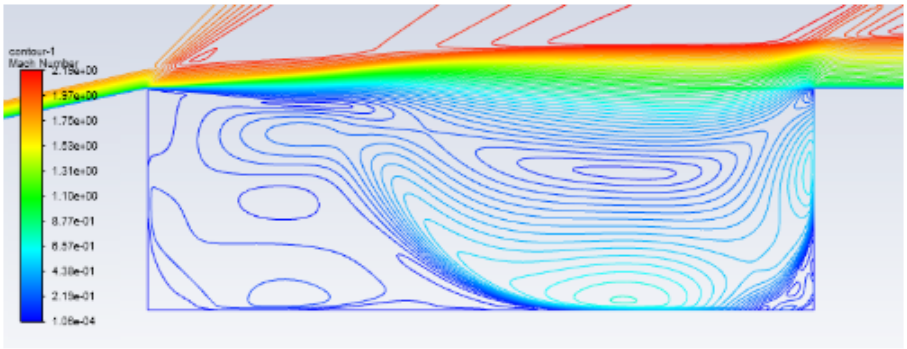

Fig. 5: Mach Contour of L/D = 3

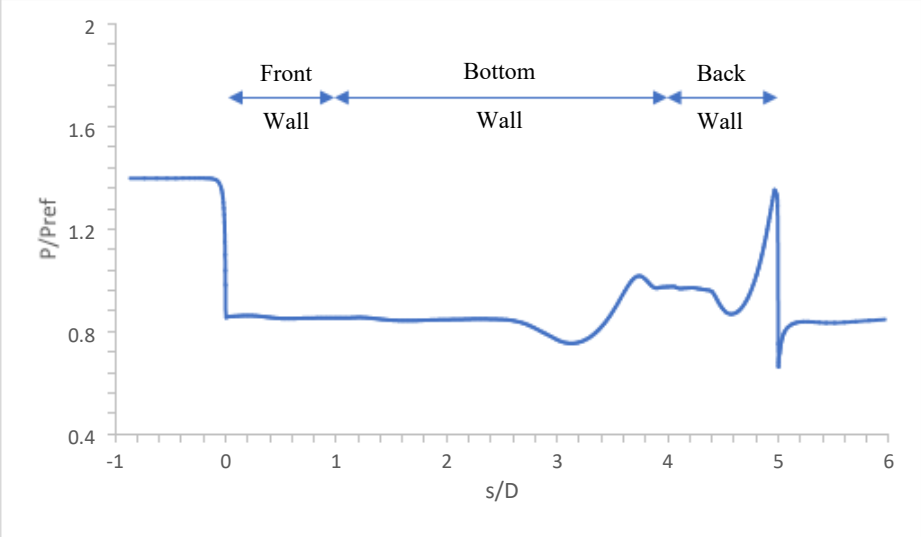

Fig. 6: Pressure Distribution for L/D = 3

Fig. 7: Static Pressure Contour of L/D = 3

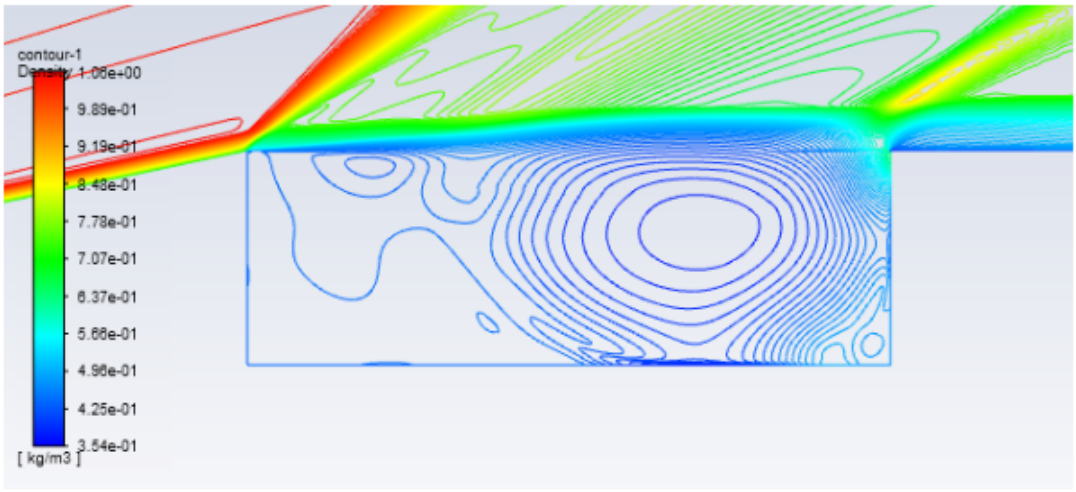

Fig. 8: Density Contour of L/D = 3

Simulations were executed for the axisymmetric cavity of L/D = 1 as well by making a similar grid with same contours and mean static pressure distribution are given in Fig. 6, 7, 8 and 9 respectively. Here, <s/D<1 represents front wall surface, 1<s/D<2 represents cavity bottom surface and 2<s/D<3 represents cavity rear wall. In this case, the value of peak pressure is 1.2348 which is lesser than L/D = 3.

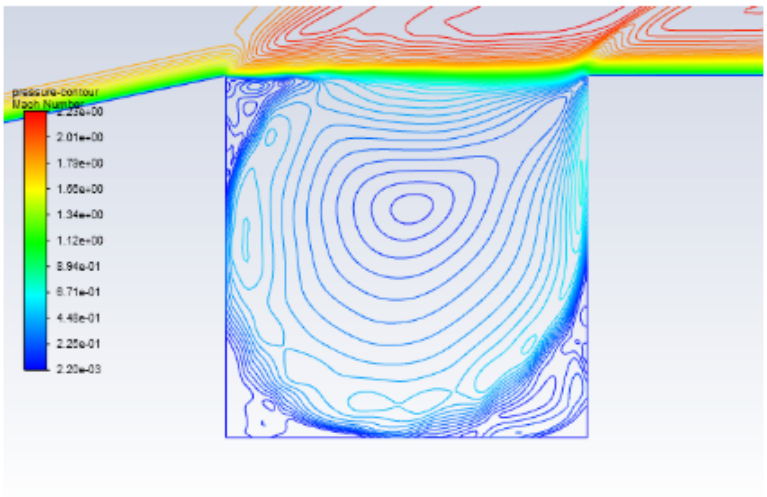

Fig. 9: Mach Contour of L/D = 1

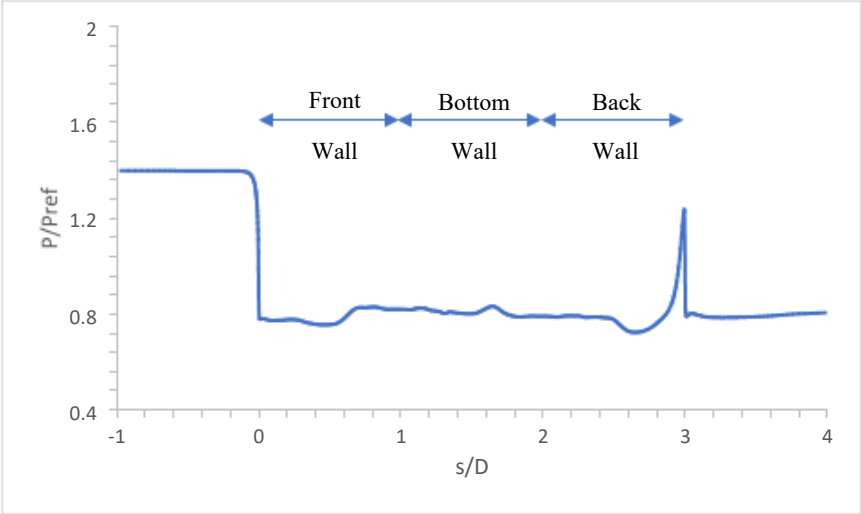

Fig. 10: Static Pressure Distribution for L/D = 1

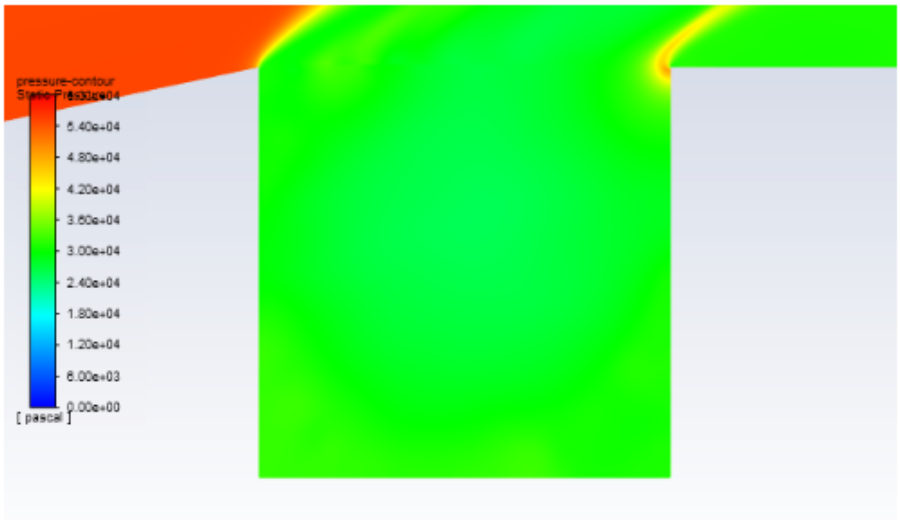

Fig. 11: Static Pressure Contour of L/D = 1

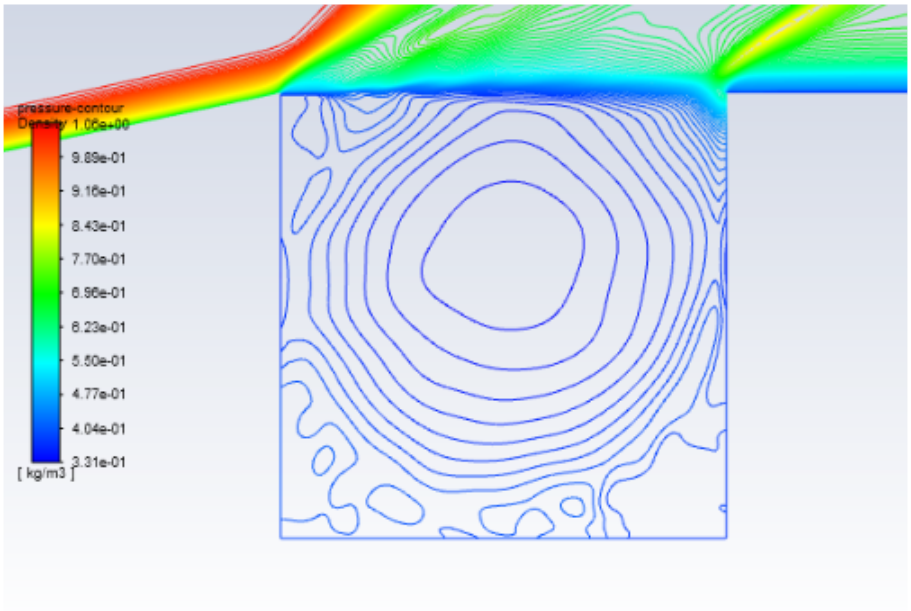

Fig. 12: Density Contour of L/D = 1

Simulations were further executed to procure the consequence of angle of attack on both the cavities. In this project, angle of attack was varied as 10°, 5° and 3°. The distribution of mean static pressure on the upper cavity section and lower cavity section changes because by varying the angle of attack, the geometry of those sections is no longer same. Value of mean static pressure in the upper cavity section is lesser than that of lower cavity section. As we increase the angle of attack, mean static pressure elevates in the lower cavity section. Although in the upper cavity section, it first increases, but as the angle of attack is further escalated, mean static pressure diminishes in the upper cavity section. Pressure fluctuations on the rear wall tip were also captured during the transient simulations and as the angle of attack was elevating, pressure fluctuations on both upper and lower cavity sections were decreased. Mean static pressure distribution curve for both L/D = 1 and L/D = 3 are given below.

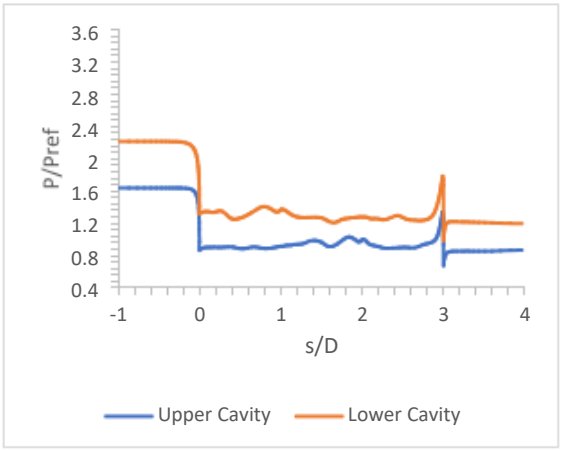

(a)

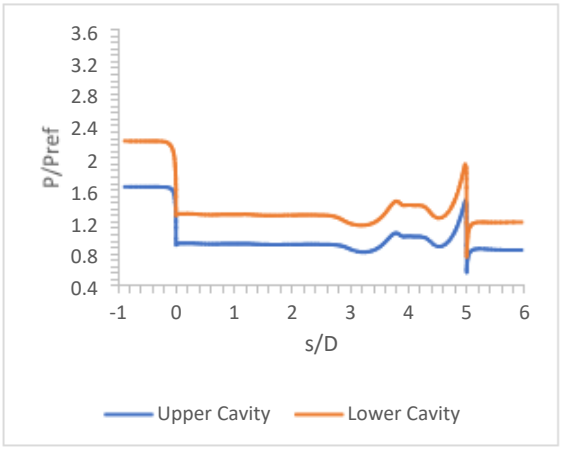

(a)

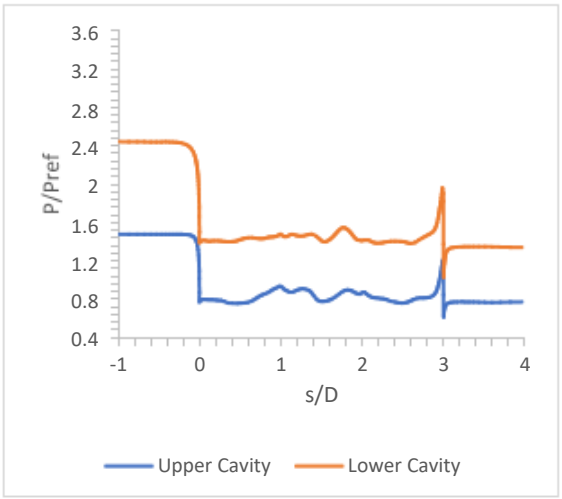

(b)

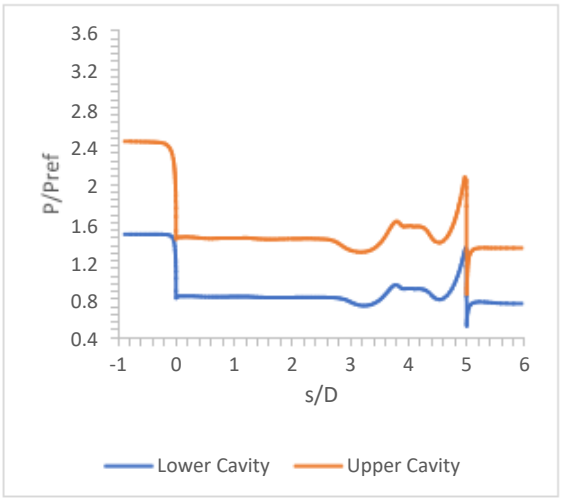

(b)

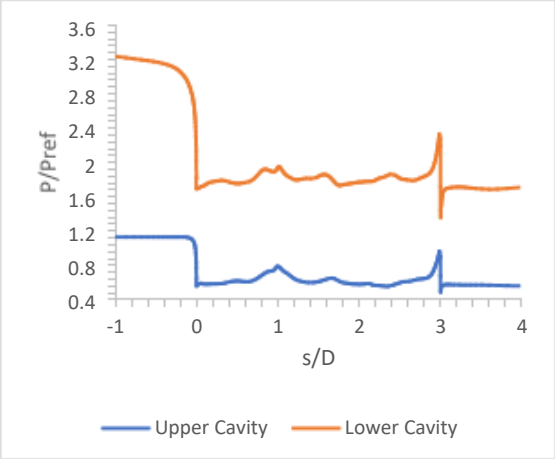

(c)

Fig. 13: Static Pressure Distribution for L/D = 1 **(a)** α = 3° **(b)** α = 5° **(c)** α = 10°

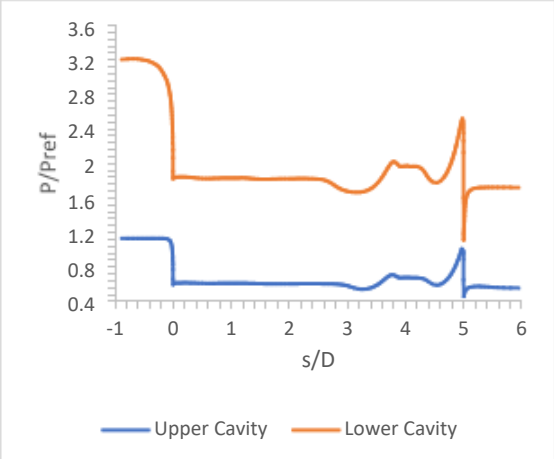

(c)

Fig. 14: Static Pressure Distribution for L/D = 3 **(a)** α = 3° **(b)** α = 5° **(c)** α = 10°

A juxtaposition of distribution of mean static pressure in upper cavity and lower cavity at different angles of attack for both L/D = 1 and L/D = 3 are presented below.

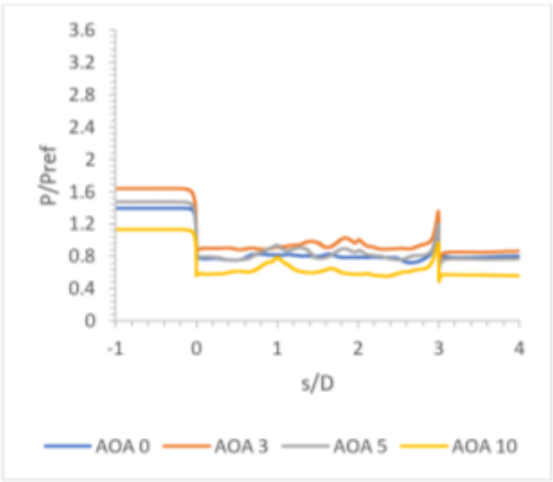

(a)

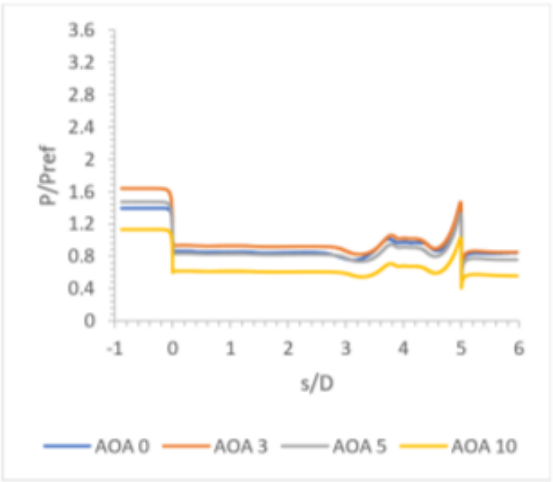

(a)

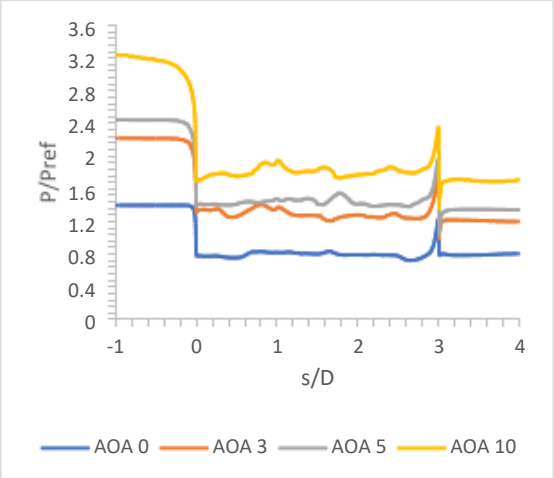

(b)

Fig. 15: Static Pressure Distribution for L/D = 1 in **(a)** Upper Cavity Section **(b)** Lower Cavity Section

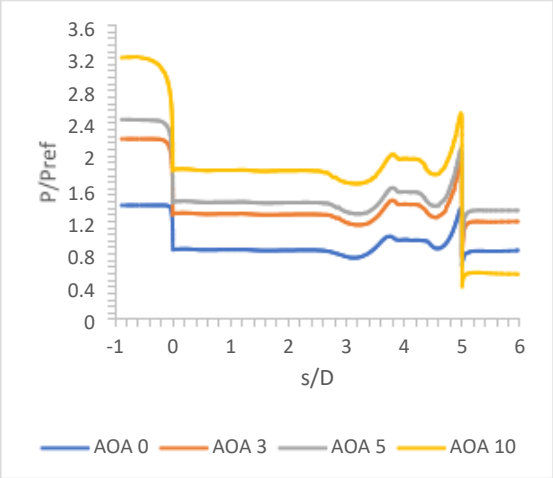

(b)

Fig. 16: Static Pressure Distribution for L/D = 3 in **(a)** Upper Cavity Section **(b)** Lower Cavity Section

A comparison of peak pressure on the rear wall at all angles of attack in upper and lower cavity section for both L/D = 1 and L/D = 3 are given in the below figures and tables.

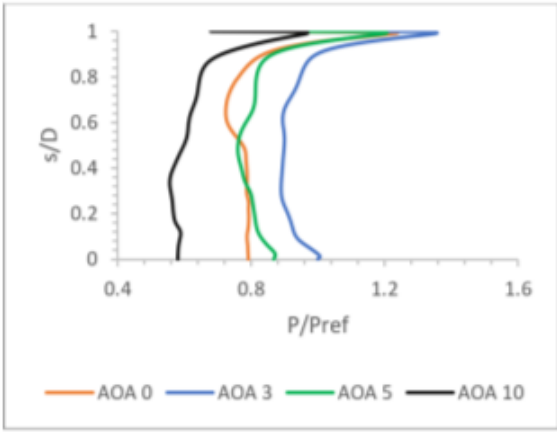

(a)

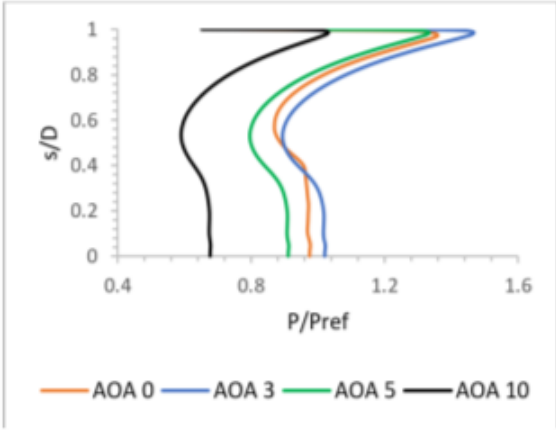

(a)

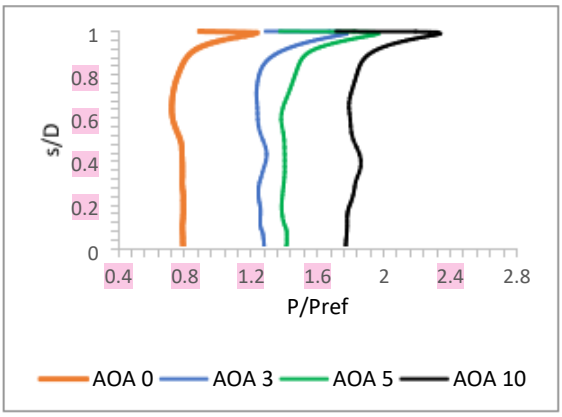

(b)

Fig. 17: Comparison of static pressures on rear wall for L/D = 1 in **(a)** Upper Cavity Section **(b)** Lower Cavity Section

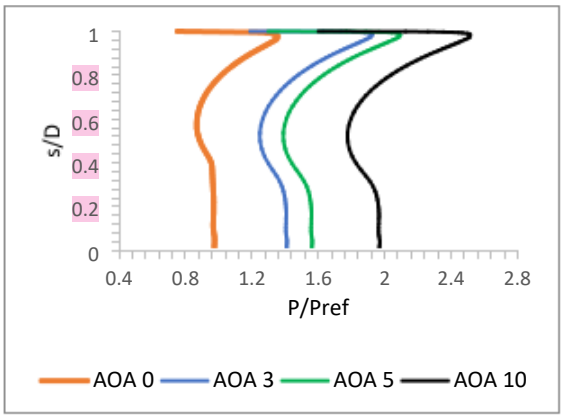

(b)

Fig. 18: Comparison of static pressures on rear wall for L/D = 3 in **(a)** Upper Cavity Section **(b)** Lower Cavity Section

Table 1: Change in peak pressure at different α

Angle of Attack (°)	Change in peak pressure in L/D = 1 (%)		Change in peak pressure in L/D = 3 (%)	
	Upper Cavity	Lower Cavity	Upper Cavity	Lower Cavity
3	9.97	44.74	8.00	41.63
5	-2.21	59.90	-1.95	54.08
10	-21.58	90.28	-24.13	85.28

Clearly, from the above table and figures, there is about 22% decrease in the peak pressure on the rear wall at 10° angle of attack in the upper cavity section in case of L/D = 1 and about 24% decrease in case of L/D = 3.

Pressure fluctuations on the rear wall tip are represented underneath. In case of L/D = 1, collective mode periodic oscillations were distinguished in all three angles of attack, but in L/D = 3, oscillations were there however, they were non-periodic in nature. Fluctuations in both the cases are reduced as the angle of attack is increased, but fluctuations in L/D = 3 are so low that it does not make much difference.

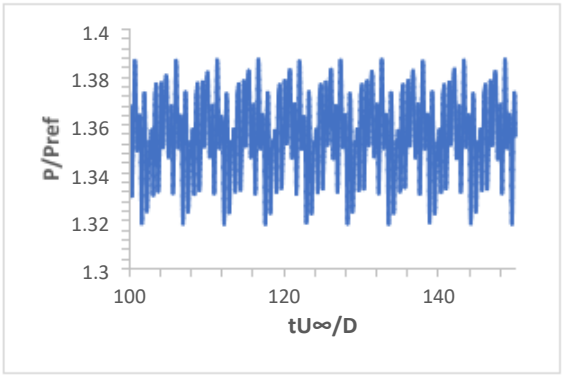

(a)

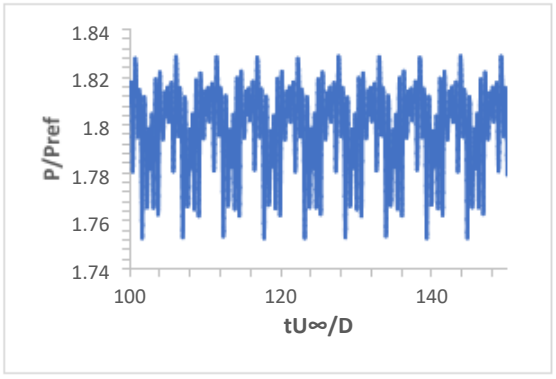

(a)

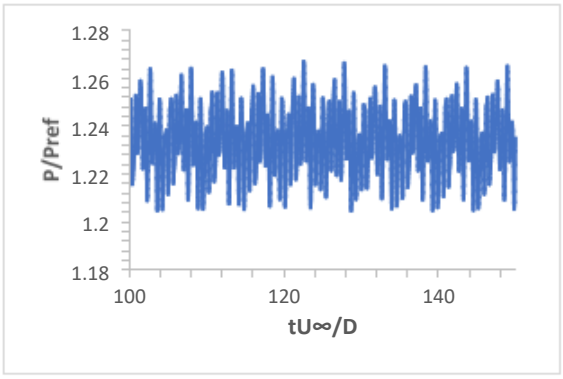

(b)

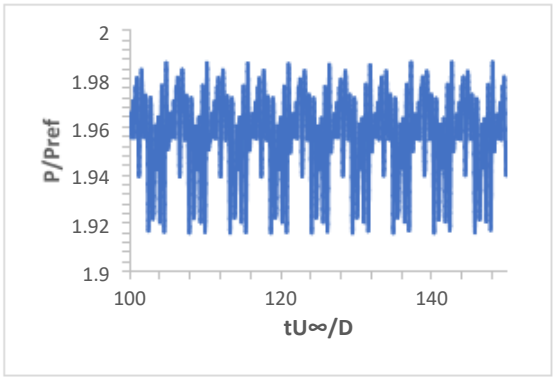

(b)

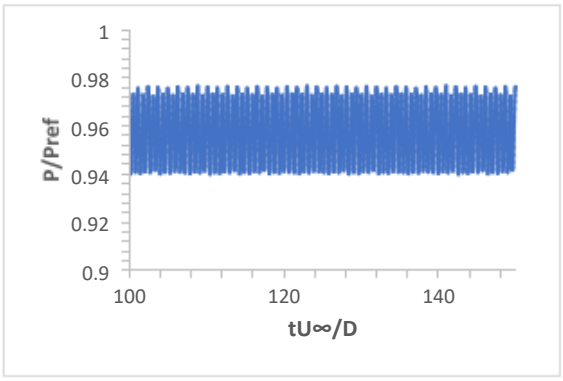

(c)

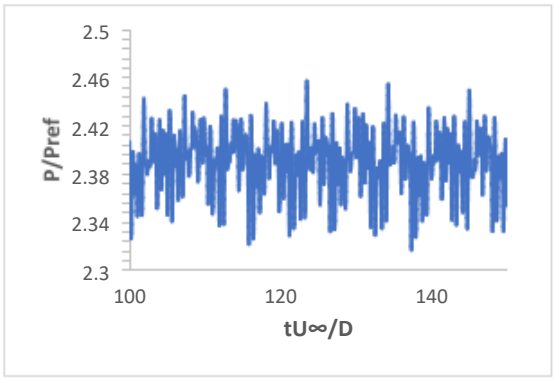

(c)

Fig. 19: Pressure time history in upper cavity of L/D = 1 at **(a)** α = 3° **(b)** α = 5° **(c)** α = 10°

Fig. 20: Pressure time history in lower cavity of L/D = 1 at **(a)** α = 3° **(b)** α = 5° **(c)** α = 10°

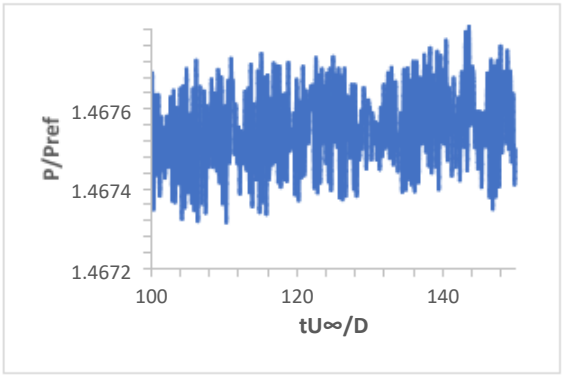

(a)

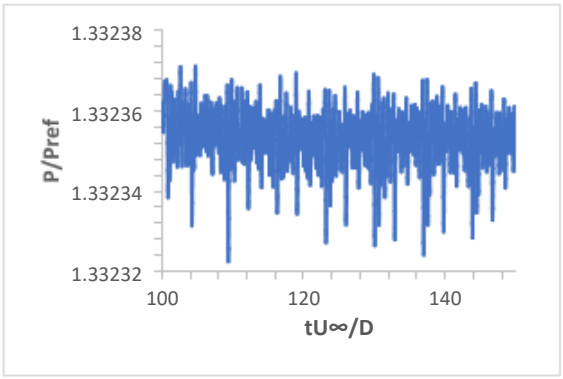

(b)

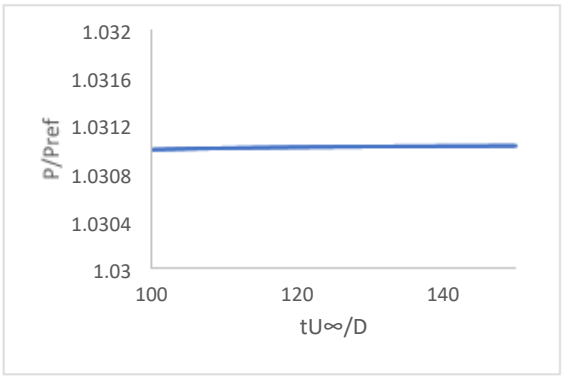

(c)

Fig. 21: Pressure time history in upper cavity of L/D = 3 at **(a)** α = 3° **(b)** α = 5° **(c)** α = 10°

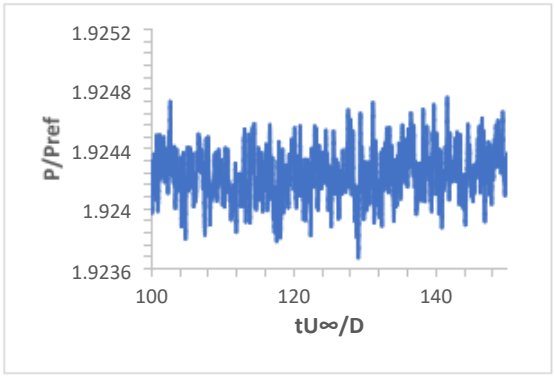

(a)

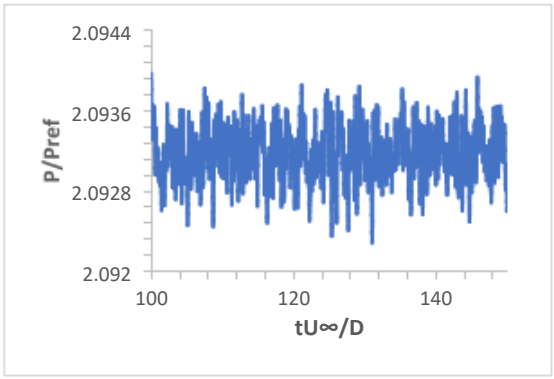

(b)

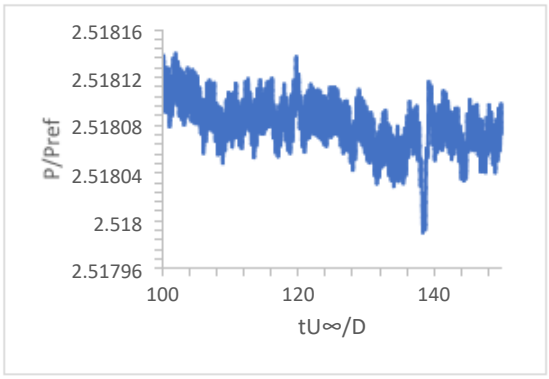

(c)

Fig. 22: Pressure time history in upper cavity of L/D = 3 at **(a)** α = 3° **(b)** α = 5° **(c)** α = 10°

CONCLUSION

Simulations were accomplished to attain flow field details around axisymmetric cavities of L/D = 2 and L/D = 3 at Mach 2.0. Studies were made by varying angle of attack (α) of the cavity. It was done by changing the direction of flow at inlet boundary condition in the ANSYS FLUENT setup. Angle of attack was diversified and its effect on overall distribution of pressure inside the cavity and pressure fluctuations on the rear wall was investigated. Results indicate a significant reduction in peak pressure in the upper cavity section at 10° angle of attack. Also, by observing the distribution of pressure of the lower cavity section and comparing it with that of upper cavity section in Fig. 12 and 13, it can be observed that flow separation occurs quickly in lower cavity section. As the angle of attack was increased, pressure fluctuations also reduced marginally in the upper cavity section.